

Breakdown of thermalization in finite one-dimensional systems

Marcos Rigol

Department of Physics, Georgetown University, Washington, DC 20057, USA

We use quantum quenches to study the dynamics and thermalization of hardcore bosons in finite one-dimensional lattices. We perform exact diagonalizations and find that, far away from integrability, few-body observables thermalize. We then study the breakdown of thermalization as one approaches an integrable point. This is found to be a smooth process in which the predictions of standard statistical mechanics continuously worsen as the system moves toward integrability. We establish a direct connection between the presence or absence of thermalization and the validity or failure of the eigenstate thermalization hypothesis, respectively.

PACS numbers: 03.75.Kk, 03.75.Hh, 05.30.Jp, 02.30.Ik

Little more than fifty years ago, Fermi, Pasta, and Ulam (FPU) [1] set up a numerical experiment to prove the ergodic hypothesis for a one-dimensional (1D) lattice of harmonic oscillators once nonlinear couplings were added. Much to their surprise, the system exhibited long-time periodic dynamics with no signals of ergodicity. This behavior could not be explained in terms of Poincaré recurrences and motivated intense research [2], which ultimately gave rise to the modern chaos theory. It led to the discovery of solitons (stable solitary waves) in nonlinear systems and to the understanding of thermalization in terms of dynamical chaos [2]. In the latter scenario, there is a threshold below which the interactions breaking integrability are ineffective in producing chaotic behavior and the system cannot be described by standard statistical mechanics [3]. The FPU numerical calculations happened to be below that threshold [4].

More recently, experiments with ultracold gases in 1D geometries have challenged our understanding of the quantum domain [5]. After bringing a nearly isolated system out of equilibrium, no signals of relaxation to the expected thermal equilibrium distribution were observed. Some insight can be gained in the framework of integrable quantum systems [6], but then it remains the question of why thermalization did not occur even when the system was supposed to be away from integrability. In the latter regime, thermalization is expected to occur [7, 8]. This new experimental result [5] has opened many questions such as: Will thermalization occur if one waits longer? Is there a threshold after which thermalization will occur? In this work we address some of these questions using numerical experiments.

In the limit in which the quantum system is integrable, it has been shown numerically [6] that observables such as the ones measured experimentally relax to an equilibrium distribution different from the thermal one. That a novel distribution is generated is the result of the conserved quantities that render the system integrable, and can be characterized by a generalization of the Gibbs ensemble (GGE) [6]. Several works since then have addressed the relevance and limitations of the GGE to various integrable systems and classes of observables [9]. Much less is known away from integrability where fewer analytical tools are available and numerical computations become more demanding. Early works in 1D have provided mixed re-

sults; thermalization was observed in some regimes and not in others [10]. In two dimensions, thermalization was unambiguously shown to occur [8] and could be understood on the basis of the eigenstate thermalization hypothesis [7]. Recent works have also pointed out a possible intermediate quasi-steady regime that could occur before thermalization in a class of fermionic systems [11]. Here we study how breaking integrability affects the thermalization of correlated bosons in a 1D lattice after a quantum quench.

We consider impenetrable bosons in a periodic 1D lattice with nearest-neighbor hopping t and repulsive interaction V , and next-nearest-neighbor hopping t' and repulsive interaction V' . The Hamiltonian reads [12]

$$\hat{H} = \sum_{i=1}^L \left\{ -t \left(\hat{b}_i^\dagger \hat{b}_{i+1} + \text{H.c.} \right) + V \left(\hat{n}_i - \frac{1}{2} \right) \left(\hat{n}_{i+1} - \frac{1}{2} \right) - t' \left(\hat{b}_i^\dagger \hat{b}_{i+2} + \text{H.c.} \right) + V' \left(\hat{n}_i - \frac{1}{2} \right) \left(\hat{n}_{i+2} - \frac{1}{2} \right) \right\}. \quad (1)$$

When $t' = V' = 0$ this model is integrable. In order to understand how the proximity to the integrable point affects equilibration, we prepare an initial state that is an eigenstate of a system with $t = t_{ini}$, $V = V_{ini}$, t' , V' and then quench the nearest-neighbor parameters to $t = t_{fin}$, $V = V_{fin}$ without changing t' , V' , i.e., we only change $t_{ini}, V_{ini} \rightarrow t_{fin}, V_{fin}$. The same quench is then repeated for different values of t', V' as one approaches $t' = V' = 0$. We have performed the exact time evolution of up to eight impenetrable bosons in lattices with up to 24 sites. Taking advantage of translational invariance, this required the full diagonalization of blocks in the Hamiltonian that contained up to 30,667 states.

Does integrability, or its absence, affect the relaxation dynamics of experimentally relevant observables? To answer that question, we examine two of those observables: the momentum distribution function $n(k)$ and the structure factor for the density-density correlations $N(k)$ [12]. Since the initial state wavefunction can be expanded in the eigenstate basis of the final Hamiltonian \hat{H} as $|\psi_{ini}\rangle = \sum_{\alpha} C_{\alpha} |\Psi_{\alpha}\rangle$, one finds that, if the spectrum is nondegenerate and incommensurate, the infinite time average of an observable \hat{O} can be written as

$$\overline{\langle \hat{O} \rangle} \equiv O_{diag} = \sum_{\alpha} |C_{\alpha}|^2 O_{\alpha\alpha}, \quad (2)$$

where $O_{\alpha\alpha}$ are the matrix elements of \hat{O} in the basis of the final Hamiltonian. This exact result can be thought as the prediction of a “diagonal ensemble”, where $|C_\alpha|^2$ is the weight of each state of this ensemble [8]. We then study the normalized area between our observables, during the time evolution, and their infinite time average, i.e., at each time we compute

$$\delta n_k = \frac{\sum_k |n(k) - n_{diag}(k)|}{\sum_k n_{diag}(k)} \quad (3)$$

and similarly for δN_k . If, up to small fluctuations, $n(k)$ and $N(k)$ relax to a constant distribution, it must be the one predicted by the infinite time average in Eq. (2), i.e., $\delta n(k), \delta N(k) \rightarrow 0$.

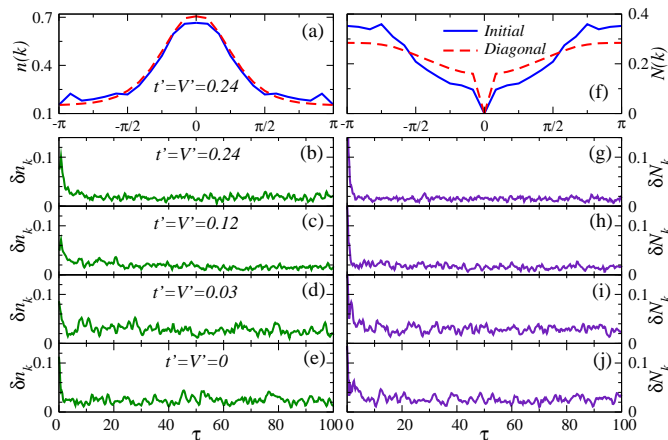


FIG. 1: Quantum quench from $t_{ini} = 0.5$, $V_{ini} = 2.0$ to $t_{fin} = 1.0$, $V_{fin} = 1.0$, with $t'_{ini} = t'_{fin} = t'$ and $V'_{ini} = V'_{fin} = V'$ in a system with eight hardcore bosons ($N_b = 8$) in 24 lattice sites ($L = 24$). The initial state was chosen within the eigenstates of the initial Hamiltonian with total momentum $k = 0$ in such a way that after the quench the system has an effective temperature $T = 2.0$ in all cases. Given the energy of the initial state in the final Hamiltonian $E = \langle \psi_{ini} | \hat{H}_{fin} | \psi_{ini} \rangle$ the effective temperature is computed as described in Ref. [13]. (a) Initial and diagonal ensemble results for $n(k)$ when $t' = V' = 0.24$. (b)–(e) Time evolution of δn_k for $t' = V' = 0.24$, 0.12, 0.03, and 0.0 respectively. (f) Initial and diagonal ensemble results for $N(k)$ when $t' = V' = 0.24$. (g)–(j) Time evolution of δN_k for $t' = V' = 0.24$, 0.12, 0.03, and 0.0 respectively.

In Fig. 1, we show results for δn_k and δN_k as a function of time τ for four different quenches as one approaches the integrable point. In Figs. 1(a) and 1(f), we compare the initial $n(k)$ and $N(k)$ with the predictions of Eq. (2) away from integrability. Interestingly, the time evolution of δn_k and δN_k in Figs. 1(b)–1(e) and Figs. 1(g)–1(j), respectively, can be seen to be very similar for all values of t' and V' . Hence, the dynamics are barely affected by the closeness to the integrable point [12]. In all cases, we find that there is a fast relaxation of $n(k)$ and $N(k)$ towards the diagonal ensemble prediction (in a time scale $\tau \sim 1/t_{fin}$ [12]) and that later they fluctuate within one to two percent of that prediction. The latter differences decrease as one increases the system size and the energy, or the effective temperature [13] of the system [12]. From these results, we infer that, for very large systems sizes

and finite effective temperatures, $n(k)$ and $N(k)$ should in general relax to exactly the predictions of Eq. (2) even if the system is very close or at integrability.

Once it is known that the diagonal ensemble provides a very good description of observables after their relaxation dynamics, a question that remains to be answered is how good are standard statistical ensembles in reproducing the $n(k)$ and $N(k)$ distributions predicted by the diagonal ensemble as one approaches the integrable point? Based on the experimental results [5] one would expect conventional statistical mechanics to fail everywhere in 1D or at least over a finite window in the vicinity of the integrable point. We find the latter scenario to be the one realized in our finite 1D lattices.

In the main panel of Fig. 2(a), we compare the diagonal ensemble results with the predictions of the microcanonical ensemble for our two observables of interest. We find the differences between them to be below one percent and de-

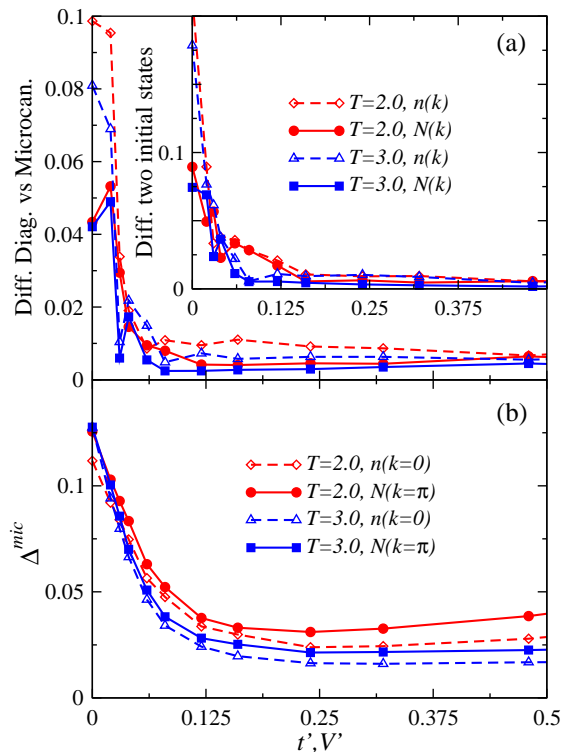


FIG. 2: Comparison between the predictions of different statistical ensembles for $n(k)$ and $N(k)$ after relaxation in a system with $L = 24$ and $N_b = 8$. Results are shown for $T = 2.0$ and $T = 3.0$. (a) (main panel) Relative difference between the predictions of the diagonal ensemble and the microcanonical ensemble. (a) (inset) Relative difference between the predictions of two diagonal ensembles generated by different initial states selected from the eigenstates of a Hamiltonian with $t_{ini} = 0.5$, $V_{ini} = 2.0$ and a Hamiltonian with $t_{ini} = 2.0$, $V_{ini} = 0.5$, and $L = 24$, $N_b = 8$. The final Hamiltonian ($t_{fin} = 1.0$, $V_{fin} = 1.0$) and the effective temperature are identical for both initial states. Relative differences are computed following Eq. (3). (b) Average relative deviation of eigenstate expectation values with respect to the microcanonical prediction (see text) as a function of t', V' , for the same effective temperatures as in (a).

creasing with system size [12] when the system is far from integrability ($t' = V' > 0.1$). Thus, one can say that thermalization takes place in this case. As one approaches the integrable point, on the other hand, the differences between the diagonal and microcanonical ensembles increase, signaling a breakdown of thermalization in 1D. This breakdown is accompanied by a dependence of the properties of the system after relaxation on the initial state, as can be seen in the inset in Fig. 2(a). There, we compare the predictions of the diagonal ensemble for two different initial states that have the same effective temperature. Those predictions are almost independent of the initial state for $t' = V' > 0.1$, but strongly dependent on it closer to integrability. In Fig. 2(a), it is remarkable to find that both $n(k)$ and $N(k)$ exhibit very similar quantitative behavior away from integrability, which is an indication of the generality of our results for few-body observables.

A clarification is in order at this point. It is usually assumed that, for extensive quantities, the predictions of conventional statistical mechanical ensembles such as the microcanonical and canonical ones are identical, provided the systems are large enough. We should stress that this is not the case in our small systems, and may not be the case for many experiments that are performed in similar setups. In Fig. 3 one can see that depending on the physical observable under consideration the differences between the predictions of those ensembles can be quite large [in particular for $n(k)$]. Interestingly, they are almost not affected by the proximity to integrability, and, as expected, can be seen to reduce with increasing system size.

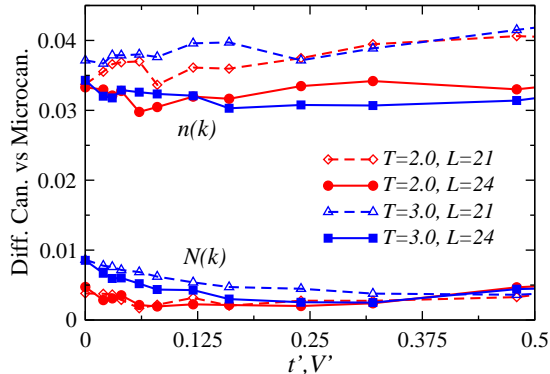


FIG. 3: Relative difference between the predictions of the microcanonical and canonical ensembles for our two observables of interest in systems with $L = 21$, $N_b = 7$ and $L = 24$, $N_b = 8$. Relative differences are computed following Eq. (3).

One may wonder why conventional statistical mechanical ensembles can predict the exact values of few-body observables after relaxation at all, since these seem to be a priori fully dependent on the initial conditions through the values of $|C_\alpha|^2$ [see Eq. (2)]. In the main panel in Fig. 4(b), we show the distribution of $|C_\alpha|^2$ for one of the quenches that exhibited thermalization in Fig. 2(a). Figure 4(b) shows that the $|C_\alpha|^2$ distribution is clearly different from the microcanonical one, in which all states within an energy window are taken with the same weight. One can conclude then that something else is at play here.

A resolution to this puzzle was advanced by Deutsch and Srednicki in terms of the eigenstate thermalization hypothesis (ETH) [7]. ETH states that the fluctuation of eigenstate expectation values of generic few-body observables [$O_{\alpha\alpha}$ in Eq. (2)] is small between eigenstates that are close in energy, which means that the microcanonical average is identical to the prediction of each eigenstate, or what is the same that the eigenstates already exhibit a thermal value of the observable. If this holds, thermalization in an isolated quantum system will follow for any distribution of $|C_\alpha|^2$, as long as it is narrow enough in energy. This scenario was shown to be valid in isolated two-dimensional systems in Ref. [8].

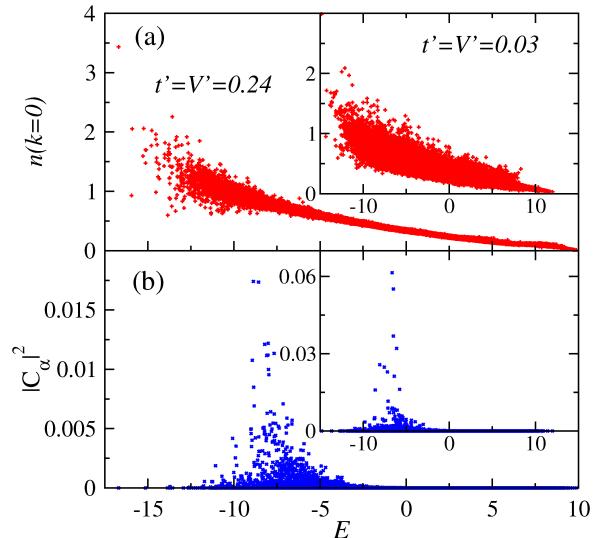


FIG. 4: (a) $n(k = 0)$ as a function of the energy for all the eigenstates of the Hamiltonian (including all momentum sectors). (main panel) $t = V = 1$ and $t' = V' = 0.24$. (inset) $t = V = 1$ and $t' = V' = 0.03$. The system has 24 lattice sites and 8 bosons for which the total Hilbert space consists of 735,471 states. (b) Distribution of $|C_\alpha|^2$ for the quench from $t_{ini} = 0.5$, $V_{ini} = 2.0$ to $t_{fin} = 1.0$, $V_{fin} = 1.0$ for an effective temperature $T = 2.0$. (main panel) $t = V = 1$ and $t' = V' = 0.24$, where $E = \langle \psi_{ini} | \hat{H}_{fin} | \psi_{ini} \rangle = -6.85$. (inset) $t = V = 1$ and $t' = V' = 0.03$, where $E = -5.95$.

In 1D systems, we find the onset of thermalization to be directly related to the validity of the eigenstate thermalization hypothesis. In the main panel in Fig. 4(a), we depict $n(k = 0)$ [similar results were obtained for $n(k \neq 0)$ and $N(k)$] in each eigenstate of the Hamiltonian as a function of the energy of the eigenstate, when the system is far from integrability. Figure 4(a) shows that after a region of low energies where the eigenstate expectation values exhibit large fluctuations follows another region where fluctuations are small and ETH holds. The inset in Fig. 4(a) shows that for a system close to the integrable point, in which thermalization is absent [Fig. 2(a)], the eigenstate to eigenstate fluctuations of $n(k = 0)$ are very large over the entire spectrum and ETH does not hold.

In order to be more quantitative, and to understand how ETH breaks down as one approaches the integrable point, we have computed the average relative deviation of the eigenstate

expectation values with respect to the microcanonical prediction (Δ^{mic}) for $n(k=0)$ and for $N(k=\pi)$ [12]. They are shown in Fig. 5(a) and 5(b), respectively, as a function of the effective temperature T corresponding to an energy E of the microcanonical ensemble [13]. Temperature in this plot is only used as an auxiliary tool for assessing how far from the ground state these systems are.

In Fig. 5 one can see that $\Delta^{mic}n(k=0)$ and $\Delta^{mic}N(k=\pi)$ exhibit very similar behavior. Below $T \simeq 1.5$ fluctuations are large and due to the relatively small number of states in some energy windows the use of the microcanonical ensemble may not be well justified. For $T \gtrsim 1.5$, the fluctuations saturate with increasing temperature, and $\Delta^{mic}n(k=0)$ and $\Delta^{mic}N(k=\pi)$ continuously increase, at any given temperature, as one approaches the integrable point. The latter is better seen in Fig. 2(b) for the two specific effective temperatures studied in Fig. 2(a). A comparison between Fig. 2(a) and Fig. 2(b), allows us to establish a direct connection between the breakdown of thermalization in 1D and the increase of the eigenstate to eigenstate fluctuations in the Hamiltonian, or what is the same, the failure of ETH. We have also studied how these results are modified when changing the system size. We find that for our lattice sizes Δ^{mic} still reduces as one increases the system size [12]. The relative reduction is more pronounced away from integrability.

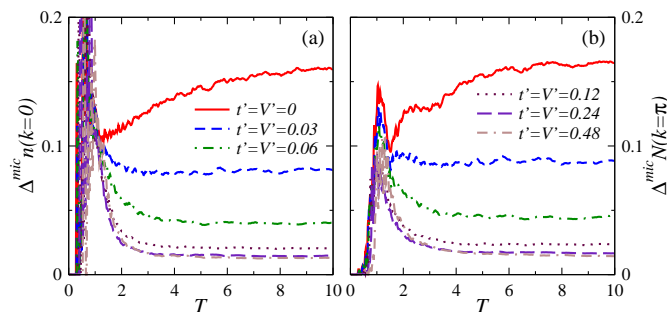


FIG. 5: Average relative deviation of eigenstate expectation values with respect to the microcanonical prediction as a function of the effective temperature of the microcanonical ensemble. Results are presented for: (a) $n(k=0)$ and (b) $N(k=\pi)$. These systems have 24 lattice sites, 8 bosons, and $t=V=1.0$. An effective temperature $T=2$ in these plots corresponds to an energy $E_{mic} = -5.95$ for $t'=V'=0.03$ and $E_{mic} = -6.85$ for $t'=V'=0.24$ and, $T=10$ corresponds to an energy $E_{mic} = -0.81$ for $t'=V'=0.03$ and $E_{mic} = -0.82$ for $t'=V'=0.24$ (see the corresponding parts of the spectrum in Fig. 4).

Overall, our study shows that in finite 1D systems there is a regime close to integrability where thermalization fails to occur, and that this failure originates in the breakdown of ETH. We also find that ETH holds further departing from integrability explaining why thermalization can occur in 1D. Since both experiments [5] and computations have been performed with relatively small systems, an important question that remains open is whether for sufficiently large system sizes thermalization will occur arbitrarily close to the integrable point or

whether there will be a finite critical value starting from which integrability breaking terms will produce thermalization. For our finite systems all we see is a smooth breakdown of thermalization as one approaches integrability [14]. The answer to this question may be well suited for experimental analysis as it may be easier to study the scaling with system size in experiments than within our numerical computations, which scale exponentially with the system size. The addition of a lattice along the 1D tubes in the experiments [16] may help in addressing these issues.

This work was supported by startup funds from Georgetown University and by the US Office of Naval Research Award No. N000140910966. We are grateful to Maxim Olshanii for discussions and useful comments on the manuscript.

-
- [1] E. Fermi, J. Pasta, and S. Ulam, Los Alamos Report LA-1940 (1955).
 - [2] See, e.g., Focus Issue: The ‘‘Fermi-Pasta-Ulam’’ Problem-The First 50 Years, *Chaos* **15**, 015101 (2005).
 - [3] B. V. Chirikov, *J. Nucl. Energy, Part C* **1**, 253 (1960).
 - [4] F. M. Izrailev, A. I. Khisamutdinov, and B. V. Chirikov, Los Alamos Report LA-4440-TR (1970).
 - [5] T. Kinoshita, T. Wenger, and D. S. Weiss, *Nature* **440**, 900 (2006).
 - [6] M. Rigol *et al.*, *Phys. Rev. Lett.* **98**, 050405 (2007); M. Rigol, A. Muramatsu, and M. Olshanii, *Phys. Rev. A* **74**, 053616 (2006).
 - [7] J. M. Deutsch, *Phys. Rev. A* **43**, 2046 (1991); M. Srednicki, *Phys. Rev. E* **50**, 888 (1994).
 - [8] M. Rigol, V. Dunjko, and M. Olshanii, *Nature* **452**, 854 (2008).
 - [9] M. A. Cazalilla, *Phys. Rev. Lett.* **97**, 156403 (2006); P. Calabrese and J. Cardy, *J. Stat. Mech.* P06008 (2007); M. Cramer *et al.*, *Phys. Rev. Lett.* **100**, 030602 (2008); T. Barthel and U. Schollwöck, *Phys. Rev. Lett.* **100**, 100601 (2008); M. Eckstein and M. Kollar, *Phys. Rev. Lett.* **100**, 120404 (2008); M. Kollar and M. Eckstein, *Phys. Rev. A* **78**, 013626 (2008); M. Cramer *et al.*, *Phys. Rev. Lett.* **101**, 063001 (2008); D. Rossini *et al.*, *Phys. Rev. Lett.* **102**, 127204 (2009). A. Iucci and M. A. Cazalilla, arXiv:0903.1205.
 - [10] C. Kollath, A. M. Läuchli, and E. Altman, *Phys. Rev. Lett.* **98**, 180601 (2007); S. R. Manmana *et al.*, *Phys. Rev. Lett.* **98**, 210405 (2007).
 - [11] M. Moeckel and S. Kehrein, *Phys. Rev. Lett.* **100**, 175702 (2008); arXiv:0903.1561; M. Eckstein, M. Kollar, and P. Werner, *Phys. Rev. Lett.* **103**, 056403 (2009).
 - [12] See supplementary material.
 - [13] Given an energy E , the effective temperature T is defined by the expression $E = Z^{-1} \text{Tr} \left\{ \hat{H} \exp(-\hat{H}/k_B T) \right\}$, where \hat{H} is the Hamiltonian for which E is measured, $Z = \text{Tr} \left\{ \exp(-\hat{H}/k_B T) \right\}$, and k_B is the Boltzmann constant. The trace runs over the full spectrum.
 - [14] Its relation with the crossover between Poissonian and Wigner-Dyson level statistics is discussed in Ref. [15].
 - [15] L. F. Santos and M. Rigol, (to be published).
 - [16] B. Paredes *et al.*, *Nature* **429**, 277 (2004).

Supplementary material for EPAPS Breakdown of thermalization in finite one-dimensional systems.

Marcos Rigol

Department of Physics, Georgetown University, Washington, DC 20057, USA

Hamiltonian and Numerical Calculations

In a system of units where $\hbar = 1$, the Hamiltonian for our model of impenetrable bosons (hardcore bosons) in a one-dimensional lattice with periodic boundary conditions reads

$$\hat{H} = \sum_{i=1}^L \left\{ -t \left(\hat{b}_i^\dagger \hat{b}_{i+1} + \text{H.c.} \right) + V \left(\hat{n}_i - \frac{1}{2} \right) \left(\hat{n}_{i+1} - \frac{1}{2} \right) - t' \left(\hat{b}_i^\dagger \hat{b}_{i+2} + \text{H.c.} \right) + V' \left(\hat{n}_i - \frac{1}{2} \right) \left(\hat{n}_{i+2} - \frac{1}{2} \right) \right\}. \quad (4)$$

where the hardcore boson creation and annihilation operators at site i are denoted by \hat{b}_i^\dagger and \hat{b}_i , respectively, and the local density operator by $\hat{n}_i = \hat{b}_i^\dagger \hat{b}_i$. In different sites the creation and annihilation operators commute as usual for bosons:

$$[\hat{b}_i, \hat{b}_j^\dagger] = [\hat{b}_i, \hat{b}_j] = [\hat{b}_i^\dagger, \hat{b}_j^\dagger] = 0, \quad \text{for } i \neq j. \quad (5)$$

However, on the same site the hardcore bosons operators satisfy anticommutation relations typical of fermions:

$$\{\hat{b}_i, \hat{b}_i^\dagger\} = 1, \quad \hat{b}_i^{\dagger 2} = \hat{b}_i^2 = 0. \quad (6)$$

These constraints avoid double or higher occupancy of the lattice sites. In Eq. (4), the nearest and next-nearest-neighbor hopping parameters are denoted by t and t' , the nearest and next-nearest-neighbor interactions are denoted by V and V' , which in our study are always repulsive, i.e., $V, V' > 0$, and L is the number of lattice sites.

For $t' = V' = 0$, the above Hamiltonian is integrable. It also exhibits a superfluid to insulator transition at half-filling as V is increased [$(V/t)_c = 2$]. Finite values of t' and V' break integrability and generate a plethora of competing phases. All our results in this work are obtained for quenches within the superfluid phase.

For our exact study of the nonequilibrium dynamics, we perform a full diagonalization of the many-body Hamiltonian (4) taking advantage of the translational symmetry of the lattice. Our initial state is always selected from the zero total momentum sector. The largest $k = 0$ sector in our study corresponds to eight bosons in 24 lattice sites, where matrices of dimension $D = 30,667$ are diagonalized. Since our quenches do not break translational symmetry only states with $k = 0$ are required for the time evolution, and we use all of them

$$|\psi(\tau)\rangle = e^{-i\hat{H}\tau} |\psi_{ini}\rangle = \sum_{\alpha} C_{\alpha} e^{-iE_{\alpha}\tau} |\Psi_{\alpha}^0\rangle,$$

where $|\psi(\tau)\rangle$ is the time-evolving state, $|\psi_{ini}\rangle$ is the initial state, $|\Psi_{\alpha}^0\rangle$ are the eigenstates of the Hamiltonian with zero total momentum and energy E_{α} , and $C_{\alpha} = \langle \Psi_{\alpha}^0 | \psi_{ini} \rangle$.

The observables of interest in this work are the momentum distribution function of the bosons

$$\hat{n}(k) = \frac{1}{L} \sum_{i,j} e^{-k(i-j)} \hat{b}_i^\dagger \hat{b}_j,$$

which is generally measured in ultracold gases experiments, and the density-density correlation structure factor

$$\hat{N}(k) = \frac{1}{L} \sum_{i,j} e^{-k(i-j)} \hat{n}_i \hat{n}_j.$$

Since we always work at a fixed number of particles N_b , the expectation value of $\hat{N}(k = 0)$ is trivially $\langle \hat{N}(k = 0) \rangle = N_b^2/L$. We subtract this trivial constant in all our plots.

Studying a one-body and a two-body observable allows us to assess the generality of our results for generic few-body observables in generic one-dimensional systems.

Relaxation Dynamics after a Quantum Quench

In Fig. 1 (main text), we have shown results for the relaxation dynamics of a system with 8 bosons ($N_b = 8$) in 24 lattice sites ($L = 24$). The initial state was selected so that the time evolving system has an effective temperature $T = 2.0$. [Given the energy of the time evolving state in the final Hamiltonian, which is conserved $E = \langle \psi_{ini} | \hat{H}_{fin} | \psi_{ini} \rangle$, the effective temperature T is defined by the expression $E = Z^{-1} \text{Tr} \left\{ \hat{H}_{fin} \exp(-\hat{H}_{fin}/k_B T) \right\}$, where \hat{H}_{fin} is the final Hamiltonian, $Z = \text{Tr} \left\{ \exp(-\hat{H}_{fin}/k_B T) \right\}$, and k_B the Boltzmann constant. The trace runs over the full spectrum, including all momentum sectors.] In Fig. 6, we present results for a quench with exactly the same Hamiltonian parameters as in Fig. 1 (main text) but taking a different initial state so that the energy of the system is higher, corresponding to an effective temperature $T = 3.0$. (Notice that for all our results $t_{fin} = 1.0$ sets the energy scale.)

Overall, we find that the time scale over which relaxation occurs is of the order $\tau \sim 1/t_{fin}$ in all cases studied. The short time scale behavior can be better seen in the insets in Fig. 6(g)-6(i). In addition, the results in Fig. 6, for an effective $T = 3.0$, show that the values of δn_k and δN_k after relaxation are slightly smaller and fluctuate less than the ones obtained for an effective temperature $T = 2.0$ [Fig. 1 (main text)]. This implies that increasing the energy of the final state improves the convergence towards the infinite time average prediction.

This difference can be understood in terms of a higher number of eigenstates of the Hamiltonian that participate during the nonequilibrium dynamics as the energy of the time-evolving state is increased. Since more states are involved, dephasing is more effective and time fluctuations after relax-

ation are smaller in these finite systems. The higher participation can be understood as the density of states increases with increasing energy, so that in general there are more states available close to any given energy the higher the latter is.

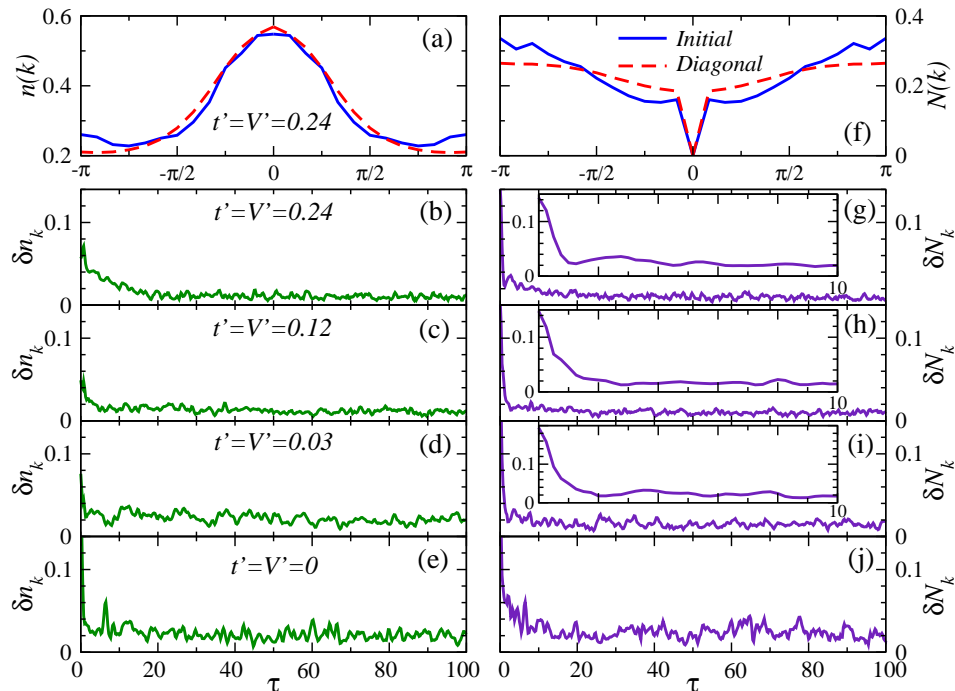


FIG. 6: Quantum quench from $t_{ini} = 0.5$, $V_{ini} = 2.0$ to $t_{fin} = 1.0$, $V_{fin} = 1.0$, with $t'_{ini} = t'_{fin} = t'$ and $V'_{ini} = V'_{fin} = V'$ in a system with eight hardcore bosons ($N_b = 8$) in 24 lattice sites ($L = 24$). The initial state was chosen within the eigenstates of the initial Hamiltonian with total momentum $k = 0$ in such a way that after the quench the system has an effective temperature $T = 3.0$ in all cases (see text). (a) Initial and diagonal ensemble results for $n(k)$ and $t' = V' = 0.24$. (b)–(e) Time evolution of δn_k for $t' = V' = 0.24, 0.12, 0.03$, and 0.0 respectively. (f) Initial and diagonal ensemble results for $N(k)$ and $t' = V' = 0.24$. (g)–(j) Time evolution of δN_k for $t' = V' = 0.24, 0.12, 0.03$, and 0.0 respectively. (g)–(i) (insets) Magnification of the short-time scales for the time evolution depicted in the main panels.

In Fig. 7, we depict the number of states that have a value of $|C_\alpha|^2$ greater than 10^{-5} , 10^{-4} , \dots , 0.1 , when the effective temperature is 2.0 [Fig. 7(a)] and 3.0 [Fig. 7(b)]. One can see there that the number of states with $|C_\alpha|^2 > 10^{-5}$, $|C_\alpha|^2 > 10^{-4}$, and $|C_\alpha|^2 > 10^{-3}$ is larger for $T = 3.0$ than for $T = 2.0$ (notice that this is a log-log plot). Since $\sum_\alpha |C_\alpha|^2 = 1$, this means that at lower temperatures there are more states with larger values of $|C_\alpha|^2$, but since those are very few in any case, dephasing tends to be less effective as the temperature decreases.

The same argument that allows us to understand the effect of the effective temperature helps in understanding why at integrability, or very close to it, δn_k and δN_k exhibit larger time fluctuations and larger average values. The effect is small ($\sim 1\%$) in Fig. 1 (main text) and Fig. 6, but can be also understood by analyzing Fig. 7. There, one can see that the number of states with the largest values of $|C_\alpha|^2$ is always the largest at integrability and continuously evolves as one moves away from integrability. In Fig. 7(b) such evolution is seen to saturate for $t' = V' > 0.12$. The effect of integrability on the number of states with large $|C_\alpha|^2$ is related to the presence of additional conserved quantities, which given the initial condi-

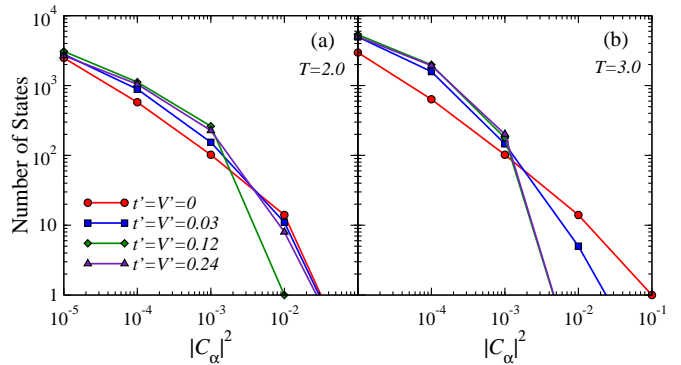


FIG. 7: Number of states with $|C_\alpha|^2$ greater than the value presented in the x axis, for an effective temperature (a) $T = 2.0$ and (b) $T = 3.0$, and for exactly same quenches studied in Fig. 1 (main text) and Fig. 6, respectively.

tions, restrict the number of states close to the energy of the system that can have a significant overlap with the initial state.

We should add that the fact that in all cases time fluctuations are found to be relatively small, even though these systems are not only finite but small, can be related to the smallness of

the off-diagonal elements of the physical observables under consideration and has been discussed before [1, 2].

Finally, the effect of changing the system size can be studied by considering a smaller system with exactly the same density and effective temperature as the one in Fig. 6. Results for a system with 7 hardcore bosons in 21 lattice sites are depicted in Fig. 8. They exhibit a qualitatively similar behavior

to the one seen in Fig. 6, but after relaxation δn_k and δN_k show larger time fluctuations and the values around which they fluctuate are also larger than for the system with $N_b = 8$ and $L = 24$. This supports the expectation that for sufficiently large system sizes time fluctuations after relaxation will be arbitrarily small and relaxation will occur towards the exact predictions of the diagonal ensemble.

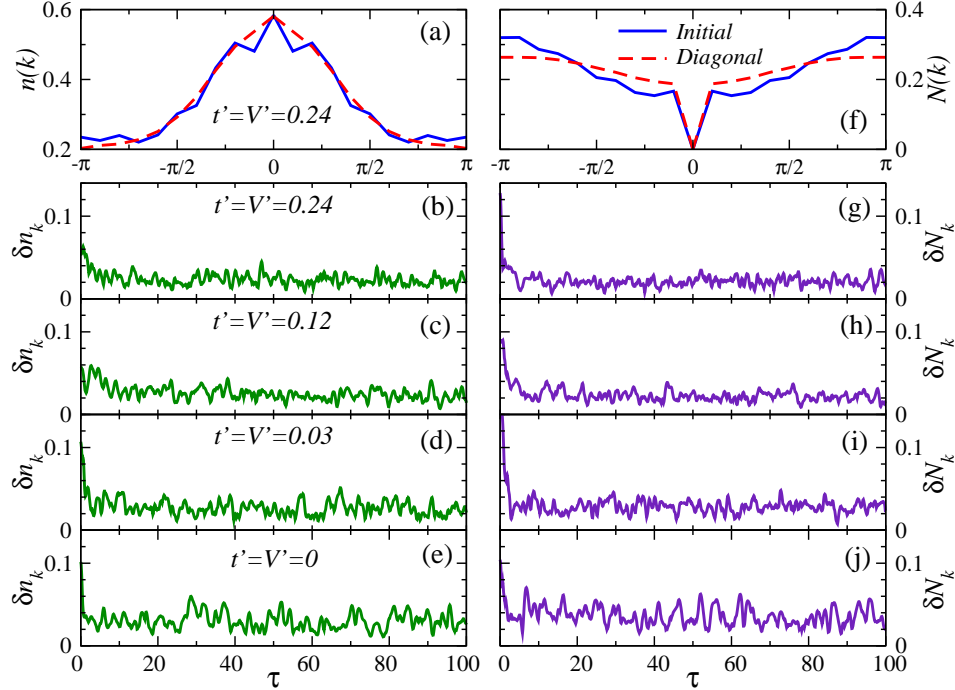


FIG. 8: Quantum quench from $t_{ini} = 0.5$, $V_{ini} = 2.0$ to $t_{fin} = 1.0$, $V_{fin} = 1.0$, with $t'_{ini} = t'_{fin} = t'$ and $V'_{ini} = V'_{fin} = V'$ in a system with $N_b = 7$ and $L = 21$. The initial state was chosen within the eigenstates of the initial Hamiltonian with total momentum $k = 0$ in such a way that after the quench the system has an effective temperature $T = 3.0$ in all cases (see text), as was done for Fig. 6. (a) Initial and diagonal ensemble results for $n(k)$ and $t' = V' = 0.24$. (b)–(e) Time evolution of δn_k for $t' = V' = 0.24, 0.12, 0.03$, and 0.0 respectively. (f) Initial and diagonal ensemble results for $N(k)$ and $t' = V' = 0.24$. (g)–(j) Time evolution of δN_k for $t' = V' = 0.24, 0.12, 0.03$, and 0.0 respectively.

The Microcanonical Ensemble

The computations of the microcanonical ensemble predictions are done averaging over all eigenstates (from all momentum sectors) that lie within a window $[E - \Delta E, E + \Delta E]$, where $E = \langle \psi_{ini} | \hat{H}_{fin} | \psi_{ini} \rangle$, and we have taken $\Delta E = 0.1$ in all cases. We have checked that our results are robust in the neighborhood of this value of ΔE . In Fig. 9, we show (a) the momentum distribution function and (b) the density-density structure factor for three different values of ΔE . The results for each observable are indistinguishable from each other. Further confirmation of this can be obtained looking at the inset in Fig. 9(a), where we depict the behavior of $n(k = 0)$ and $N(k = \pi)$ vs ΔE for $0.01 < \Delta E < 0.2$. Both quantities can be seen to be almost independent of ΔE on that window. Similar results have been obtained for all other values of t', V' considered in this work.

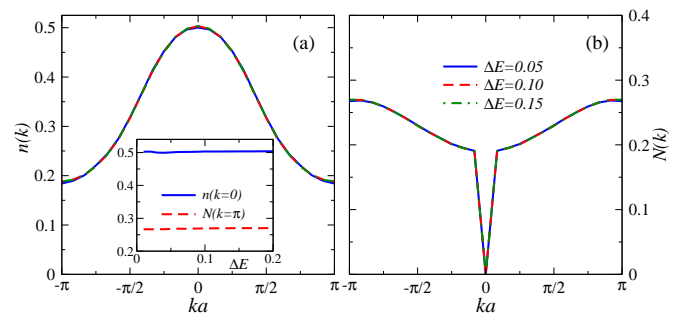


FIG. 9: (a) (main panel) Microcanonical momentum distribution function and (b) density-density structure factor for three different values of ΔE . (b) (inset) $n(k = 0)$ and $N(k = \pi)$ vs ΔE . The system has $N_b = 8$, $L = 24$, and a total energy $E = -3.87$, which corresponds to an effective temperature $T = 3.0$ for $t' = V' = 0.03$ and $t = V = 1.0$.

Different Ensembles

In Fig. 2(a) (main text), we compared the predictions of different ensembles for our two observables of interest at different effective temperatures, but the same system size $N_b = 8$ and $L = 24$. In order to gain an understanding of finite size effects, in Fig. 10 we present results for identical calculations in smaller systems with $N_b = 7$ and $L = 21$, which have the same density as the ones in Fig. 2 (main text). Overall, we find a similar qualitative behavior in these smaller systems. However, as expected, in the smaller lattices the relative differences are always larger than in the larger systems. This is particularly evident away from integrability, where in Fig. 2(a) (main text) all differences are below one percent while in Fig. 10 they are two to three times larger than that.

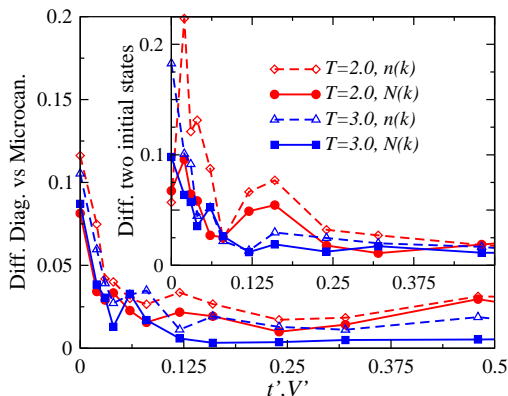


FIG. 10: Comparison between the predictions of different statistical ensembles for $n(k)$ and $N(k)$ after relaxation. Results are shown for two different effective temperatures. (a) (main panel) Relative difference between the predictions of the diagonal ensemble and the microcanonical ensemble ($L = 21$, $N_b = 7$). (a) (inset) Relative difference between the predictions of two diagonal ensembles generated by different initial states, selected from the eigenstates of a Hamiltonian with $t_{ini} = 0.5$, $V_{ini} = 2.0$ and a Hamiltonian with $t_{ini} = 2.0$, $V_{ini} = 0.5$. The final Hamiltonian ($t_{fin} = 1.0$, $V_{fin} = 1.0$) and the effective temperature are identical for both initial states.

Eigenstate Thermalization Hypothesis

In Fig. 11(a), we show the eigenstate expectation values of $n(k = 0)$ as a function of the energy of the eigenstate for a system with $L = 21$ and $N_b = 7$. The values of t , V , t' and V' in the main panel and the inset correspond to the exact same values presented in Fig. 4(a) (main text) for $L = 24$ and $N_b = 8$. The behavior of $n(k = 0)$ is very similar in both systems in which the lattice size and the total filling are the only difference, as we have kept the density constant. These results exemplify the robustness of ETH or its failure for our finite systems. Notice that in Fig. 4 (main text) and Fig. 11, we are showing results for the eigenstate expectation values of $n(k = 0)$ in the full spectrum (including all momentum sectors). The validity of ETH in the full spectrum explains why our microcanonical calculations, in which we included

the contributions from all momentum sectors, provide a correct prediction for the outcome of the diagonal ensemble even though in the latter ensemble only states with zero total momentum have a finite weight.

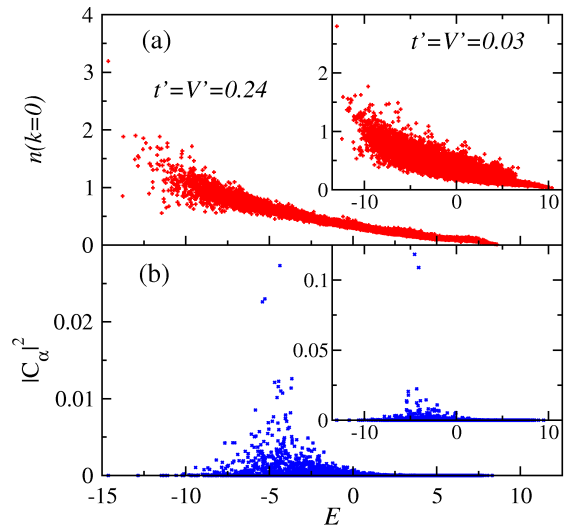


FIG. 11: (a) $n(k = 0)$ as a function of the energy for all the eigenstates of the Hamiltonian (from all momentum sectors). (main panel) $t = V = 1$ and $t' = V' = 0.24$. (inset) $t = V = 1$ and $t' = V' = 0.03$. The system has 21 lattice sites and 7 bosons for which the total Hilbert consists of 116,280 states. (b) Distribution of $|C_\alpha|^2$ for the quench from $t_{ini} = 0.5$, $V_{ini} = 2.0$ to $t_{fin} = 1.0$, $V_{fin} = 1.0$ for an effective temperature $T = 3.0$. (main panel) $t = V = 1$ and $t' = V' = 0.24$, where $E = \langle \psi_{ini} | \hat{H}_{fin} | \psi_{ini} \rangle = -3.85$. (inset) $t = V = 1$ and $t' = V' = 0.03$, where $E = \langle \psi_{ini} | \hat{H}_{fin} | \psi_{ini} \rangle = -3.44$.

In Fig. 11(b), we show the distribution of $|C_\alpha|^2$ for the same Hamiltonian parameters as in Fig. 4(b) (main text), but once again for a smaller system with $L = 21$ and $N_b = 7$, and also for a higher effective temperature of the time evolving state. In Fig. 4(b) (main text), we showed results for $T = 2.0$ and in Fig. 11(b), we are showing results for $T = 3.0$. Qualitatively, one can see that there is not much difference between those two cases. The distribution of $|C_\alpha|^2$ is in stark contrast with the weight given to each eigenstate expectation value in the microcanonical and canonical distributions. $|C_\alpha|^2$ vs E_α is a distribution that strongly depends on the initial conditions of the system, and $|C_\alpha|^2$ exhibits strong fluctuations between contiguous eigenstates. The only generic feature one can see by comparing Fig. 4(b) (main text) with Fig. 11(b) is that in both cases the distribution of $|C_\alpha|^2$ is peaked around the mean energy of the time evolving state.

Deviations from ETH

To have a quantitative understanding of how ETH breaks down as one approaches integrability, we computed the average relative deviation of the eigenstate expectation values with respect to the microcanonical prediction, $\Delta^{mic} n(k = 0)$ and

$\Delta^{mic}N(k = \pi)$. For any given energy of the microcanonical ensemble, these quantities are computed as

$$\Delta^{mic}n(k = 0) = \frac{\sum_{\alpha} |n_{\alpha\alpha}(k = 0) - n_{mic}(k = 0)|}{N_{states} n_{mic}(k = 0)} \quad (7)$$

and

$$\Delta^{mic}N(k = \pi) = \frac{\sum_{\alpha} |N_{\alpha\alpha}(k = \pi) - N_{mic}(k = \pi)|}{N_{states} N_{mic}(k = \pi)} \quad (8)$$

where $n_{\alpha\alpha}(k = 0)$ and $N_{\alpha\alpha}(k = \pi)$ are the eigenstate expectation values of $n(k = 0)$ and $N(k = \pi)$, respectively, and $n_{mic}(k = 0)$ and $N_{mic}(k = \pi)$ are the microcanonical expectation values at any given energy E . The sum over α contains all states with energies in the window $[E - \Delta E, E + \Delta E]$, and N_{states} is the number of states in the sum. As discussed before $\Delta E = 0.1$.

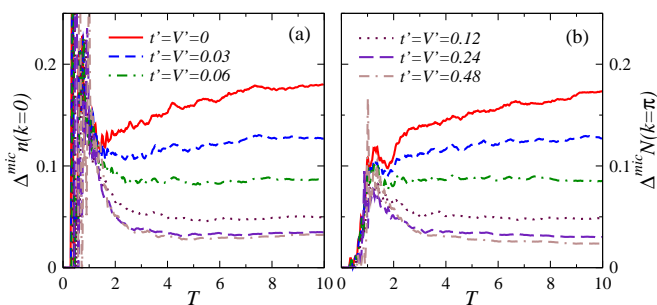


FIG. 12: Average relative deviation of eigenstate expectation values with respect to the microcanonical prediction as a function of the effective temperature of the microcanonical ensemble. Results are presented for: (a) $n(k = 0)$ and (b) $N(k = \pi)$. These systems have 21 lattice sites, 7 bosons, and $t = V = 1.0$. An effective temperature $T = 2$ in these plots corresponds to an energy $E_{mic} = -5.25$ for $t' = V' = 0.03$ and $E_{mic} = -6.05$ for $t' = V' = 0.24$ and, $T = 10$ corresponds to an energy $E_{mic} = -0.75$ for $t' = V' = 0.03$ and $E_{mic} = -0.76$ for $t' = V' = 0.24$ (see the corresponding parts of the spectrum in Fig. 11).

In order to compare results for different Hamiltonian parameters, we have plotted $\Delta^{mic}n(k = 0)$ and $\Delta^{mic}N(k = \pi)$ as a function of the effective temperature T , corresponding to an energy E of the microcanonical ensemble. Having the energy of the microcanonical ensemble E , T can be computed from $E = Z^{-1} \text{Tr} \{ \hat{H} \exp(-\hat{H}/k_B T) \}$, where $Z = \text{Tr} \{ \exp(-\hat{H}/k_B T) \}$. Notice that here this effective temperature is only used as an auxiliary tool for assessing how far from the ground state these systems are, and to have a unique

energy scale window for comparing different observables independently of the Hamiltonian parameters t' and V' , which change the ground state energy and level spacing.

Results for $\Delta^{mic}n(k = 0)$ and $\Delta^{mic}N(k = \pi)$ are shown in Fig. 12(a) and 12(b), respectively, for a system with $L = 21$ and $N_b = 7$. The results depicted in Fig. 12 are qualitatively similar to those in Fig. 5 (main text). Below $T \simeq 1.5$ fluctuations are in general large and nonmonotonic. For $T \gtrsim 1.5$, one can see that Δ^{mic} for $n(k = 0)$ and $N(k = \pi)$ continuously increase, at any given temperature, as one approaches the integrable point, i.e., there is no abrupt transition as $t', V' \rightarrow 0$.

A direct comparison between some of the results presented in Fig. 5 (main text) and Fig. 12 is depicted in Fig. 13. There, one can see that Δ^{mic} in general reduces as one increases the system size [except for $\Delta^{mic}N(k = \pi)$ when $t' = V' = 0$]. The relative change is more pronounced away from integrability. These results do not allow us to discriminate between two possible scenarios for the breakdown of thermalization in quantum systems. A first scenario in which ETH may hold arbitrarily close to the integrable point as the system size increases, and another possible scenario in which in the thermodynamic limit there may be a critical value of t', V' (the integrability breaking terms) below which ETH does not hold and above which it does. This question will need to be addressed in future works.

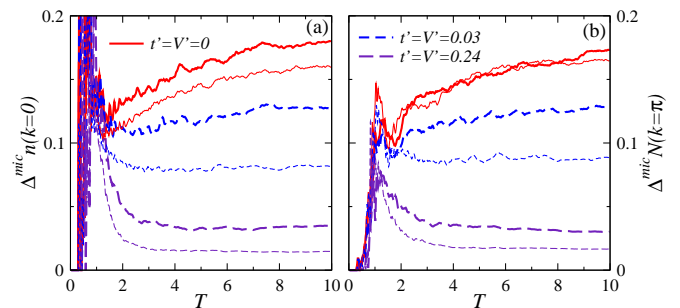


FIG. 13: Comparison between the average relative deviation of eigenstate expectation values with respect to the microcanonical prediction for two different system sizes. $L = 21$ and $N_b = 7$ (thick lines), and $L = 24$ and $N_b = 8$ (thin lines). Results are presented for: (a) $n(k = 0)$ and (b) $N(k = \pi)$. In all cases $t = V = 1.0$.

- [1] M. Srednicki, J. Phys. A **29**, L75 (1996).
 [2] M. Rigol, V. Dunjko, and M. Olshanii, Nature **452**, 854 (2008).